https://doi.org/10.5194/gmd-2022-228
Preprint. Discussion started: 10 November 2022

Geoscientific Model Development Discussions

Multidecadal and climatological surface current simulations for the southwestern Indian Ocean at 1/50° resolution

Noam Vogt-Vincent[1] and Helen Johnson[1]

[1]Department of Earth Sciences, South Parks Road, University of Oxford, Oxford, UK

Correspondence: Helen Johnson (helen.johnson@earth.ox.ac.uk)

Abstract. The **W**estern **Ind**ian Ocean **S**imulation (WINDS) is a regional configuration of the Coastal and Regional Ocean Community Model (CROCO) for the southwestern Indian Ocean. WINDS has a horizontal resolution of $1/50°$ (∼2 km) and spans a latitudinal range of 23.5° S – 0° N, and a longitudinal range from the East African coast to 77.5° E. We ran two experiments using the WINDS confugration: WINDS-M, a full 28-year multidecadal run (1993–2020); and WINDS-C, a 10-year climatological control run with monthly climatological forcing. WINDS was primarily run for buoyant Lagrangian particle tracking applications, and horizontal surface velocities are output at a temporal resolution of 30 minutes. Other surface fields are output daily, and the full 3D temperature, salinity, and velocity fields are output every 5 days. We demonstrate that WINDS successfully manages to reproduce surface temperature, salinity, currents and tides in the southwestern Indian Ocean, and is therefore appropriate for use in regional marine dispersal studies for buoyant particles, or other applications using high-resolution surface ocean properties.

1 Introduction

The western Indian Ocean is a relatively data-sparse region. Surface current data are required to simulate the dispersion of buoyant particles such as marine debris or coral larvae (van Sebille et al., 2018), and whilst global products exist that cover the southwestern Indian Ocean, derived from satellite altimetry (e.g. Rio et al., 2014) and global ocean reanalyses (e.g. Lellouche et al., 2021), these products are at a coarse resolution relative to the scales of larval dispersal and do not resolve sub-mesoscale dynamics which are thought to be important for larval transport (e.g. Monismith et al., 2018; Dauhajre et al., 2019; Grimaldi et al., 2022). Some higher-resolution models have been run in the southwestern Indian Ocean, but these simulations only spanned a limited subset of coral reefs within the region, and are not available on publicly-accessible repositories (Mayorga-Adame et al., 2016, 2017). Our objectives were to (1) provide improved estimates of regional surface currents for Seychelles, including at sub-mesoscale, (2) estimate the connectivity of reefs within Seychelles and across the wider southwestern Indian Ocean, and (3) investigate temporal variability in larval dispersal across the southwestern Indian Ocean. Bridging the gap between the fine-scale dynamics that dominate in coastal seas, and large-scale ocean currents and mesoscale variability in the high seas, is a major challenge in modelling larval dispersal (Edmunds et al., 2018). Future developments in unstructured ocean models, and improvements in the availability of computational resources, will be invaluable in addressing these challenges. However, for this study, we used a $1/50°$ (∼2 km) configuration of a regional (structured) ocean model to simulate circulation

https://doi.org/10.5194/gmd-2022-228
Preprint. Discussion started: 10 November 2022

Geoscientific Model Development Discussions

in the southwestern Indian Ocean, which we call the **W**estern **Ind**ian Ocean **S**imulation (WINDS). Here, we provide a full description of WINDS and the two experiments we ran using the configuration, and validate WINDS as relevant for buoyant Lagrangian particle tracking applications.

2 Methods

2.1 Numerics

We ran WINDS using version 1.1 of the Coastal and Regional Ocean Community Model (CROCO, http://www.croco-ocean.org/), coupled with the XIOS2.5 I/O server for writing model output (https://forge.ipsl.jussieu.fr/ioserver). WINDS uses a nonlinear equation of state (Jackett and Mcdougall, 1995; Shchepetkin and McWilliams, 2003) with a 3^{rd}-order upstream biased scheme for lateral momentum advection, a split-and-rotated 3^{rd}-order upstream biased scheme for lateral tracer advection, a 4^{th}-order compact scheme for vertical momentum advection, and a 4^{th}-order centered scheme with harmonic averaging for vertical tracer advection. Lateral momentum mixing is achieved through a Laplacian Smagorinsky parameterisation (Smagorinsky, 1963), and a Generic Length Scale $k-\epsilon$ scheme is used for vertical mixing (Jones and Launder, 1972). A bulk formulation is used for surface turbulent fluxes (`COARE3p0`) with current feedback enabled (i.e. momentum input from wind stress is relative to surface currents). The configuration uses radiative boundary conditions for forcing at the lateral boundaries (including non-tidal and tidal SSH, barotropic tidal currents and baroclinic non-tidal currents, and temperature and salinity). A 10-point cosine-shaped sponge layer is also used at the lateral boundaries for tracers and momentum. Bottom friction is implemented using quadratic friction with a log-layer drag coefficient, with $z_{0,b} = 0.02$ m, and $0.002 \leq C_d \leq 0.1$ (limits chosen for numerical stability). We used a baroclinic timestep of 90 s, with 60 barotropic steps per baroclinic step (Shchepetkin and McWilliams, 2005).

2.2 Model grid

We built the model grid using `CROCO_TOOLS` with longitudinal limits 34.62° S – 77.5° E, latitudinal limits of 23.5° S – 0° N, and a specified horizontal resolution of $1/50°$ (Figure 1). The western boundary of the domain is entirely land (East Africa). To maintain roughly even dimensions of grid cells across the domain, `CROCO_TOOLS` adjusts the meridional resolution of cells away from the equator, so the true meridional resolution of grid cells at the southern boundary of the WINDS domain is slightly finer, at around $1/55°$. The horizontal resolution of WINDS is therefore approximately 2 km, but actually ranging from 2.04 km at the southern boundary, to 2.22 km at the equator.

CROCO uses a terrain-following (s-coordinate) grid in the vertical. We used 50 vertical layers in WINDS, using a vertical stretching scheme that improves the resolution at the surface and bottom boundary layers, defined by the parameters $\theta_s = 8$, $\theta_b = 2$, and $h_c = 100$m (see the CROCO documentation for the technical explanation of these parameters). Since s-coordinates are terrain (and sea-surface) following, translating s-coordinates to depth depends on the local ocean depth (and, to a lesser extent, the sea-surface height η). The minimum and maximum ocean depth permitted in WINDS is 25m and 5250 m respec-

https://doi.org/10.5194/gmd-2022-228
Preprint. Discussion started: 10 November 2022

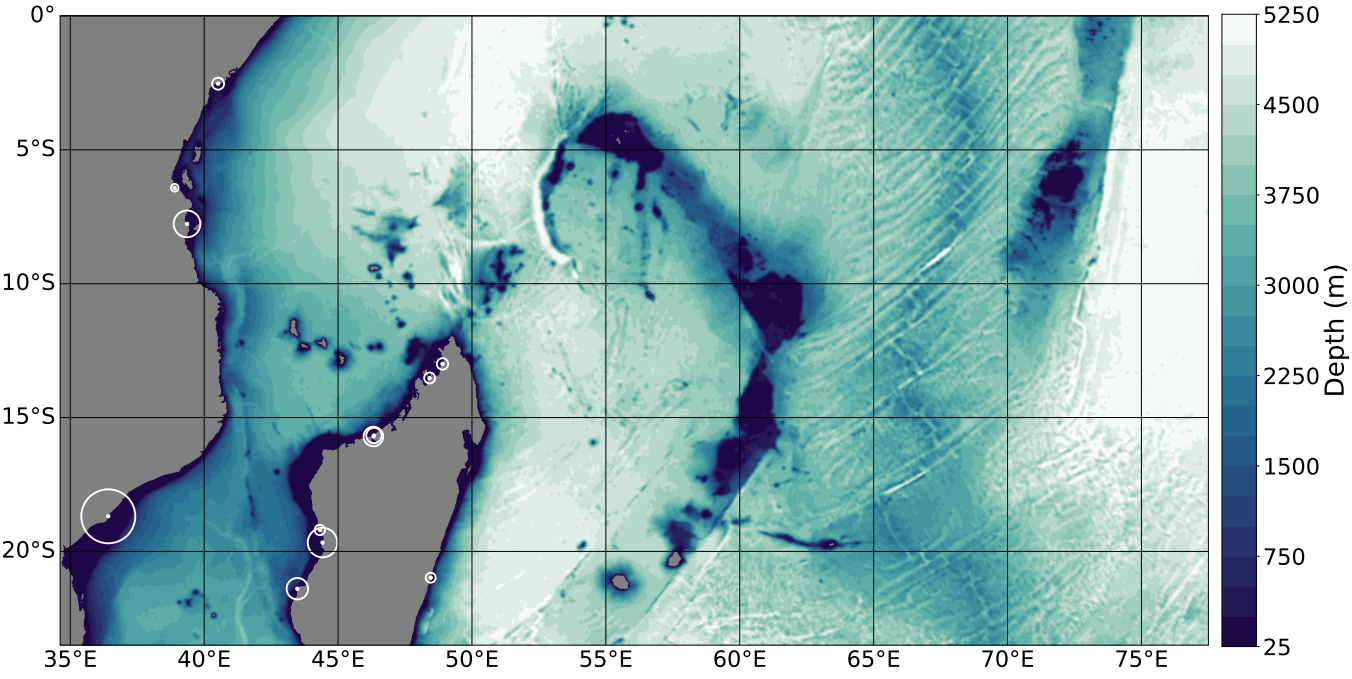

Figure 1. The entire WINDS domain, with contours representing the bathymetry used in WINDS. Circles represent the 12 rivers included in WINDS, scaled by the total annual discharge (Dai and Trenberth, 2002).

tively. For water depth of 25 m and $\eta = 0$ m, the vertical resolution is 0.40 m at the surface, 0.67 m at the sea-floor, and the coarsest vertical resolution within the water column is 0.74 m. For water depth of 5250 m, the vertical resolution is 2.07 m at the surface, 280 m at the sea-floor, and the coarsest vertical resolution within the water column is 353 m. As a result, WINDS provides excellent vertical resolution within the upper water column, particularly in shelf seas where coral reefs are.

2.3 Bathymetry

We use GEBCO 2019 (GEBCO Compilation Group, 2019) as the basis for the bathymetry in WINDS. The nominal horizontal resolution of GEBCO 2019 is 15 arc-seconds (approximately 500 m) but, due to the lack of in-situ bathymetry measurements in the southwestern Indian Ocean, most bathymetry in this region is satellite-derived, with a practical resolution of around 6km (Tozer et al., 2019). Although these satellite-derived measurements are relatively well validated, there are problems in areas of extensive continental shelves and steep bathymetry (Tozer et al., 2019). These problems are quite dramatic in the southwestern Indian Ocean. For instance, through comparison with Admiralty hydrographic navigation charts with in-situ soundings, we found local bathymetry errors in excess of 1 km around Aldabra Atoll, Seychelles, and a large number of erroneous 'islands' across Seychelles, which are in reality in significant water depth. Unfortunately, the only real solution to this lack of data is obtaining more in-situ bathymetric readings (e.g. see https://seabed2030.org/). However, to somewhat mitigate the most extreme errors in the southwestern Indian Ocean, we carried out two preprocessing steps of the GEBCO 2019 dataset. We firstly

https://doi.org/10.5194/gmd-2022-228
Preprint. Discussion started: 10 November 2022


Geoscientific Model Development Discussions

digitised all point-depth soundings from Admiralty Chart 718 (Islands North of Madagascar), including Aldabra, Assomption, Cosmoledo, Astove, and the Glorioso Islands, and then linearly gridded these data-points onto a regular 15 arc-second grid, carrying out necessary tidal adjustments, before linearly blending these grids with the rest of the GEBCO 2019 grid across a length-scale of 10-30 km. Secondly, to remove fake 'islands', we generated a land-sea mask at the GEBCO 2019 resolution from the highest resolution version of the GSHHG shoreline database (Wessel and Smith, 1996). We then set the depth of all false land cells (i.e. land according to GEBCO, ocean according to GSHHG) to 25 m. To avoid discontinuities in bathymetry, we applied a smooth $\tanh$ ramp between 25-50 m to all 'true' ocean cells shallower than 50 m (i.e. the shallower the bathymetry above 50 m, the more strongly the bathymetry would be nudged towards 50 m, with all bathymetry shallower 25 m shifted to deeper than 25 m). Although this minimum depth of 25 m is not realistic, it is a considerable improvement over a large number of fake islands, and a minimum depth of around 25 m is required for numerical stability at this resolution by CROCO anyway. As a final processing step, we carried out smoothing of bathymetry using `CROCO_TOOLS`, with a target $\nabla h/h = 0.25$ m^{-1}, to improve model stability, and reduce pressure-gradient errors in regions of steep bathymetry. The bathymetry and associated grid parameters used in all WINDS simulations can be found in the `croco_grd.nc` file in the associated datasets, and is shown in Figure 1.

2.4 Experiments: WINDS-C and WINDS-M

WINDS is forced at the surface through a bulk formulation based on ERA-5 Hersbach et al. (2020), and at the lateral boundaries with the 1/12° GLORYS12V1 global ocean reanalysis (Lellouche et al., 2021) and tides. To investigate the importance of interannual variability in circulation in the southwestern Indian Ocean, we ran two experiments within WINDS. The first, WINDS-C, is based on a monthly climatology computed from ERA-5 and GLORYS12V1 from 1993-2019. The second, WINDS-M, is based on hourly forcing from ERA-5 and daily forcing from GLORYS12V1 from 1993-2019, plus an additional year (2020) based on the associated $1/12°$ global ocean analysis (the reanalysis product for 2020 was not available at this point). It is important that WINDS-M spans multiple decades, to fully incorporate the effects of multidecadal variability in surface circulation, and therefore dispersal (Thompson et al., 2018). WINDS-C was run after a 4-year spin-up, and WINDS-M was run from the end state of WINDS-C. WINDS-C and WINDS-M are otherwise identical.

2.5 Surface forcing

Surface forcing is parameterised using a bulk formulation based on the ERA-5 global atmosphere reanalysis (Hersbach et al., 2020) at hourly (WINDS-M) or monthly climatological (WINDS-C) temporal resolution, using the following fields, bilinearly interpolated to the WINDS grid:

- Surface air temperature (`t2m`)
- Sea-surface temperature (`sst`)
- Sea-level pressure (`msl`)

https://doi.org/10.5194/gmd-2022-228
Preprint. Discussion started: 10 November 2022


Geoscientific Model Development Discussions
Open Access
EGU

- 10m wind speed (`u10`, `v10`)
- Surface wind stress (`metss`, `mntss`)
- Specific humidity (`q`)
- Relative humidity (`r`)
- Precipitation rate (`mtpr`)
- Shortwave radiation flux (`msnswrf`)
- Longwave radiation flux (`msnlwrf`)
- Downwelling longwave radiation flux (`msdwlwrf`)

Unit conversions are required for most of these quantities to put them into the form used by CROCO. Since ERA-5 is computed on a different (coarser) grid to WINDS, there is a land-sea mask mismatch between ERA-5 and WINDS. To avoid terrestrial values erroneously being applied to ocean cells in WINDS, we masked out land values from ERA-5 using the ERA-5 land-sea mask, and carried out a nearest-neighbour interpolation over the small number of coastal WINDS cells that are counted as land cells in ERA-5.

2.6 Lateral forcing

2.6.1 Ocean currents

WINDS is forced at the lateral boundaries with the $1/12°$ GLORYS12V1 global ocean reanalysis, using daily-mean (WINDS-M) or monthly-climatological (WINDS-C) depth-varying ocean current velocities, sea-surface height, temperature, and salinity. GLORYS12V1 was run using tides and, as a result, we do expect there to be aliased tidal signals remaining in the daily-mean sea-surface height fields. However, we computed that the amplitude of the strongest aliased tidal signals (both SSH and currents) should be at least $20\times$ smaller than the true tidal signals, and frequency shifted to a period of 10-30 days. As a result, we do not expect that any remnant tidal signals in GLORYS12V1 will have any significant effect on tides in WINDS.

2.6.2 Tides

WINDS is forced at the lateral boundaries with 10 tidal constituents (barotropic tidal currents and surface height) from the TPXO9-atlas (Egbert and Erofeeva, 2002): M_2, S_2, N_2, K_2, K_1, O_1, P_1, Q_1, Mf, and Mm.

2.7 Rivers

We have simplistically included 12 major rivers in WINDS: the Zambeze, Rufiji, Tsiribihina, Mangoky, Ikopa, Betsiboka, Tana, Mahavavy Nord, Sambirano, Manambolo, Mananjary, and Ruvu rivers. We assume that water in the river-mouth area

https://doi.org/10.5194/gmd-2022-228
Preprint. Discussion started: 10 November 2022


Geoscientific Model Development Discussions
Open Access
EGU

has a constant temperature of 25°C and a salinity of 15PSU, with monthly climatological discharge set according to Dai and Trenberth (2002). These riverine fluxes enter the ocean through the nearest ocean cell to the river mouth, set through inspection from satellite imagery (Google Earth). The location and annual-mean discharge of these rivers is shown in Figure 1.

3 Data Records

We have made three sets of output available from WINDS (both experiments):

- 30 minute output frequency
  - Zonal surface velocity (`u_surf`)
  - Meridional surface velocity (`v_surf`)
- 1 day output frequency
  - Sea-surface temperature (`temp_surf`)
  - Sea-surface salinity (`salt_surf`)
  - Free-surface height (`zeta`)
  - Depth-averaged zonal velocity (`u_bar`)
  - Depth-averaged meridional velocity (`v_bar`)
  - Kinematic wind stress (`wstr`)
  - Surface zonal momentum stress (`sustr`)
  - Surface meridional momentum stress (`svstr`)
  - Surface freshwater flux, E-P (`swflx`)
  - Surface net heat flux (`shflx`)
  - Net shortwave radiation at surface (`radsw`)
  - Net longwave radiation at surface (`shflx_rlw`)
  - Latent heat flux at surface (`shflx_lat`)
  - Sensible heat flux at surface (`shflx_sen`)
- 5 day output frequency
  - Zonal velocity (`u`)
  - Meridional velocity (`v`)
  - Temperature (`temp`)

https://doi.org/10.5194/gmd-2022-228
Preprint. Discussion started: 10 November 2022


Geoscientific Model Development Discussions

– Salinity (`salt`)

We did not output the vertical velocity. This can in principle be reconstructed at a 5 d frequency using the ocean depth, free-surface height, and zonal and meridional velocities.

4 Technical Validation

The following validation relates to WINDS surface properties only, as relevant for marine dispersal, since this was the primary use case WINDS-M and WINDS-C were run for. WINDS may, of course, be used for other purposes as well, but for these applications the model is provided *as is*. This validation focuses on WINDS-M, since WINDS-C is a control simulation which is not expected to fully reproduce observations as it is driven by low-frequency (monthly) climatological forcing.

4.1 Tides

We extracted the 5 largest tidal constituents (M_2, S_2, N_2, K_1, and O_1) at 50 sites across the WINDS domain (41 coastal, and 9 open-ocean) based on a 55-day 2-hourly time-series from WINDS-M 1994, and compared these amplitudes to the corresponding amplitudes in TPXO9-atlas (Egbert and Erofeeva, 2002), see Table S1. Note that this comparison is *not* independent since the TPXO9-atlas is used to set tidal boundary conditions at the WINDS domain boundaries. Additionally, TPXO9-atlas is not a purely observational product: it is a $1/30^\circ$ inverse model constrained by observations. However, TPXO9-atlas is extensively validated, and good agreement between tides in WINDS and TPXO9 does at least suggest that WINDS is propagating TPXO9-atlas tides reasonably.

Agreement between WINDS and TPXO9 is generally good, with tidal amplitude mismatch on the order of a few centimetres for almost all sites (well within the error associated with the TPXO9-atlas itself). A few regions associated with greater WINDS-TPXO9 disagreement include (1) the Sofala Bank (Mozambique) and (2) the mainland-facing sides of Mafia and Zanzibar Islands (Tanzania). Both are shelf regions with extensive shallow water and, in the case of Tanzania, complex effects from nearby islands. The roughness length scale used in the bottom friction parameterisation in WINDS is constant, and the true ocean depth at these locations is occasionally shallower than the minimum depth used in WINDS, so it is possible that a combination of these two factors could explain the poorer tidal performance of WINDS in some shelf seas.

We have also carried out a comparison of WINDS tidal predictions with selected in-situ tidal gauges spanning the longitudinal and latitudinal range of WINDS, at Mombasa (Kenya), Aldabra (Outer Islands, Seychelles), Mahé (Inner Islands, Seychelles), Diego Garcia (Chagos Archipelago), and Mauritius and Rodrigues (Mauritius) (Table 1). This comparison demonstrates that WINDS can reproduce in-situ tidal predictions well, particularly at remote islands away from extensive continental shelves.

https://doi.org/10.5194/gmd-2022-228
Preprint. Discussion started: 10 November 2022

Geoscientific Model Development Discussions

Site/Constituent	Amplitude (cm, WINDS)	Amplitude (cm, observed)
Mombasa (Kenya)		
M_2	102.8	105.5
S_2	46.7	52.1
N_2	17.8	20.1
K_1	20.8	19.1
O_1	10.5	11.3
Aldabra (Seychelles)		
M_2	94.0	93.3
S_2	47.4	46.0
N_2	16.5	17.4
K_1	16.4	16.3
O_1	8.9	10.0
Mahé (Seychelles)		
M_2	41.8	40.7
S_2	19.6	18.1
N_2	8.4	8.7
K_1	18.6	18.7
O_1	9.1	10.7
Diego Garcia (Chagos)		
M_2	47.6	49.3
S_2	28.2	28.5
N_2	8.7	8.9
K_1	3.6	3.8
O_1	3.3	3.9
Rodrigues (Mauritius)		
M_2	41.3	40.0
S_2	22.8	25.5
N_2	8.1	-
K_1	5.9	5.0
O_1	3.3	-
Mauritius (Mauritius)		
M_2	25.6	26.0
S_2	14.2	15.8
N_2	5.2	-
K_1	6.0	6.1
O_1	2.5	-

Table 1. Observational sources: Pugh (1979) (Mombasa, Aldabra, and Mahé); Lowry et al. (2009) (Rodrigues and Mauritius); Dunne (2021) (Diego Garcia).

https://doi.org/10.5194/gmd-2022-228
Preprint. Discussion started: 10 November 2022


Geoscientific Model Development Discussions

185 **4.2 Surface currents**

Figures 2–4 compare monthly climatological surface currents averaged across 1993–2020 from WINDS (left); surface currents from 1993–2020 from Copernicus GlobCurrent, combining altimetric geostrophic currents with modelled Ekman currents (centre, Rio et al. (2014)); and near-surface currents estimated from the Global Drifter Program (GDP) using drifter trajectories from 1979–2015 (right, Laurindo et al. (2017)). Both products used for comparison are entirely independent of WINDS.
190 These figures demonstrate that WINDS successively captures the location and velocity associated with major ocean currents in the southwestern Indian Ocean such as the Southern Equatorial Current, Southern Equatorial Countercurrent, North Madagascar Current, East Madagascar Current, and East African Coastal Current (e.g. Schott et al., 2009), as well as their seasonal variability. For instance, WINDS reproduces the observed strengthening of surface currents associated with the North Madagascar Current during the southeast monsoon (June-August), which can instantaneously reach approach 2 m s^{-1}, in accordance
195 with in-situ observations (Swallow et al., 1988; Voldsund et al., 2017). The East African Coast Current (EACC) also correctly strengthens dramatically during the southeast monsoon, also reaching speeds of up to (and sometimes exceeding) 2 m s^{-1}, in agreement with observations (Swallow et al., 1991; Painter, 2020). The strongest surface currents in the EACC are simulated by WINDS to be close to the equator, and can instantaneously reach 3 m s^{-1}. We are not aware of observational evidence supporting such strong surface currents within the EACC. There is a discrepancy between the strength of surface currents sim-
200 ulated by WINDS and predicted by GlobCurrent for the South Equatorial Countercurrent close to the equator (e.g. see Figure 4, November). However, this is unsurprising as GlobCurrent uses geostrophic currents, which are not defined at the equator. Agreement between WINDS and GDP-derived surface velocities are much better in this region, with WINDS reproducing observations of zonal surface currents in excess of 1 m s^{-1}, particularly towards the east of the WINDS domain (Schott and McCreary, 2001; Shao-Jun et al., 2012).

205

To assess the ability of WINDS to reproduce surface current variability associated with eddies, Figure 5 compares the eddy kinetic energy (EKE) in WINDS and Copernicus GlobCurrent (high-frequency surface currents are not available from the Global Drifter Program), as well as 8 moorings from the RAMA array (McPhaden et al., 2009; Beal et al., 2019). The spatial pattern in EKE is similar between WINDS and Copernicus GlobCurrent, with both products returning high EKE associated
210 with mesoscale eddy activity in the Mozambique Channel, around Mauritius and Réunion, in the wake of the Mascarene Plateau, and near the equator. EKE is generally higher in WINDS than Copernicus GlobCurrent, although this is likely in part due to sub-mesoscale turbulence simulated by WINDS, which will not be captured by Copernicus GlobCurrent. Compared to in-situ observations at RAMA array moorings, WINDS and Copernicus GlobCurrent tend to respectively overestimate and underestimate EKE. The RAMA time-series is considerably shorter than WINDS-M, and most moorings do not record equal
215 coverage across the seasonal cycle. However, there does not appear to be a strong seasonal cycle in EKE (Figures S1-S3), so it is unlikely that this explains the systematically higher EKE in WINDS compared to RAMA. The currents measured at RAMA are also measured at a slightly greater depth (10/12m) than WINDS (0-2m). Nevertheless, this does suggest that eddies may be too energetic in WINDS. On the other hand, the variability of daily sea-surface height (Figure 6), and therefore geostrophic

https://doi.org/10.5194/gmd-2022-228
Preprint. Discussion started: 10 November 2022

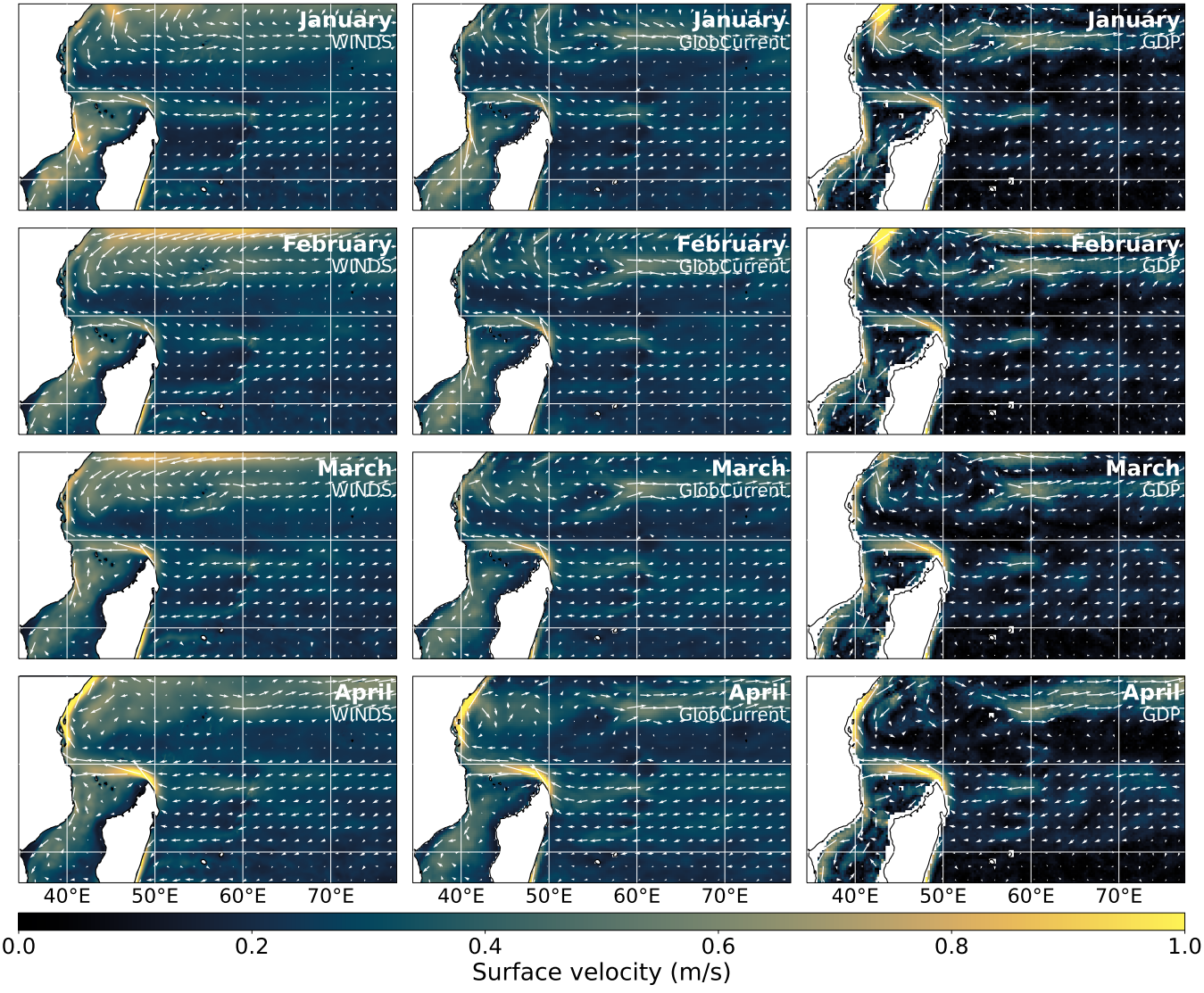

Figure 2. Monthly climatological surface currents (1993-2020) from WINDS (left), Copernicus GlobCurrent Surface (centre), and Global Drifter Program derived near-surface currents (right) for January to April.

surface currents, agrees very well with observations. This suggests that, at least away from the equator, mesoscale eddy activity is reasonably reproduced in WINDS.

4.3 Sea-surface temperature (SST) and salinity (SSS)

We have validated WINDS SST and SSS predictions by comparing monthly climatological SST and SSS from WINDS-M, to monthly climatological SST from OSTIA (Good et al., 2020) and SSS from ARMOR3D (Guinehut et al., 2012), all computed

https://doi.org/10.5194/gmd-2022-228
Preprint. Discussion started: 10 November 2022

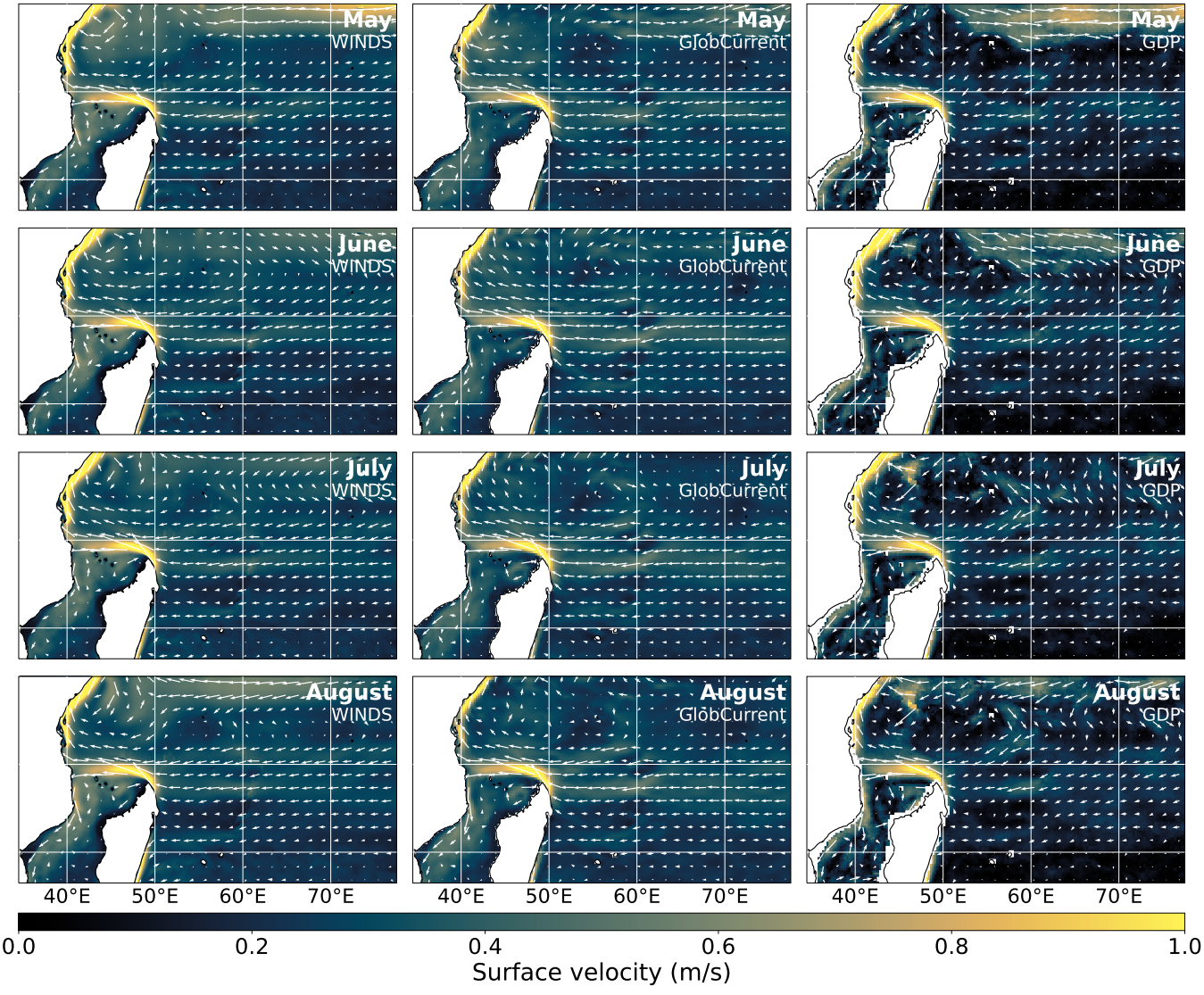

Figure 3. Monthly climatological surface currents (1993-2020) from WINDS (left), Copernicus GlobCurrent Surface (centre), and Global Drifter Program derived near-surface currents (right) for May to August.

across 1993-2020 (both are independent of WINDS, although it is important to note that observations for sea-surface salinity are sparse in the southwestern Indian Ocean). In general, WINDS performs well for both SST and SSS; the mean absolute error (MAE) for SST and SSS respectively ranges between 0.14–0.24 °C, and 0.06–0.1 PSU across the seasonal cycle (Figures 7-8). There is a widespread and year-round cold and fresh bias across most of the southwestern Indian Ocean in WINDS, although the magnitude of this bias is small. There is also a warm bias within the Mozambique Channel during the northwest monsoon (November to February), and a salty bias year-round. We do not know for certain why these biases exist in WINDS,

https://doi.org/10.5194/gmd-2022-228
Preprint. Discussion started: 10 November 2022

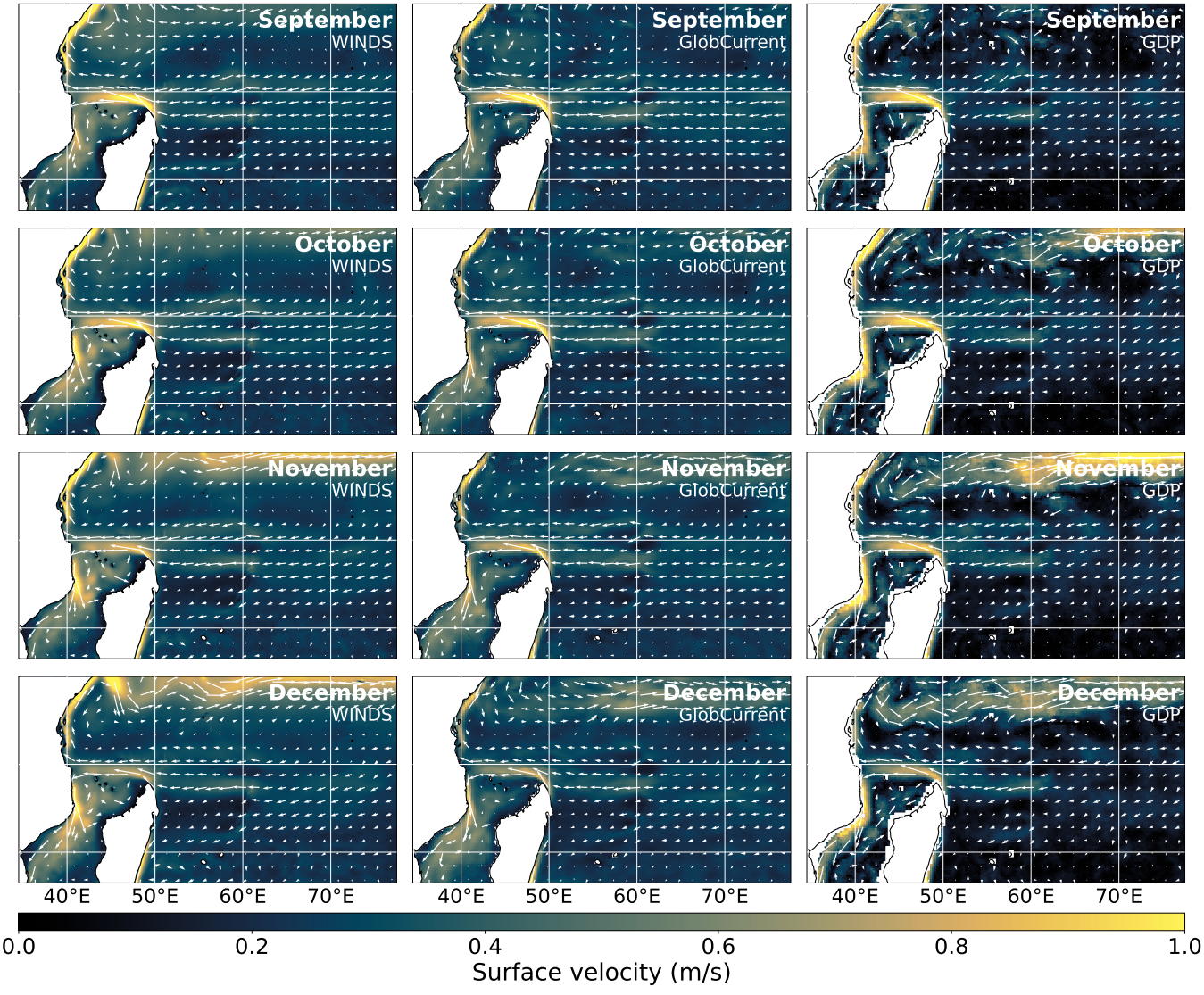

Figure 4. Monthly climatological surface currents (1993-2020) from WINDS (left), Copernicus GlobCurrent Surface (centre), and Global Drifter Program derived near-surface currents (right) for September to December.

although it may be related to the GLS vertical mixing parameterisation, resulting in an over/underestimate of the mixed-layer depth. WINDS also appears to slightly overestimate the strength of the seasonal SST cycle in shallow water along the coasts of East Africa and Madagascar. Finally, there is a spatially limited but relatively intense fresh bias in WINDS off the coast of Mozambique, associated with the Zambeze River. The implementation of rivers in WINDS is simplistic, so it is possible that the seasonal discharge climatology or physical water properties associated with the river mouth (15 PSU and 25 °C) were inappropriate, that the advection of the freshwater plume associated with the river is incorrectly simulated in WINDS, or that

https://doi.org/10.5194/gmd-2022-228
Preprint. Discussion started: 10 November 2022

Geoscientific Model Development Discussions
Open Access
EGU

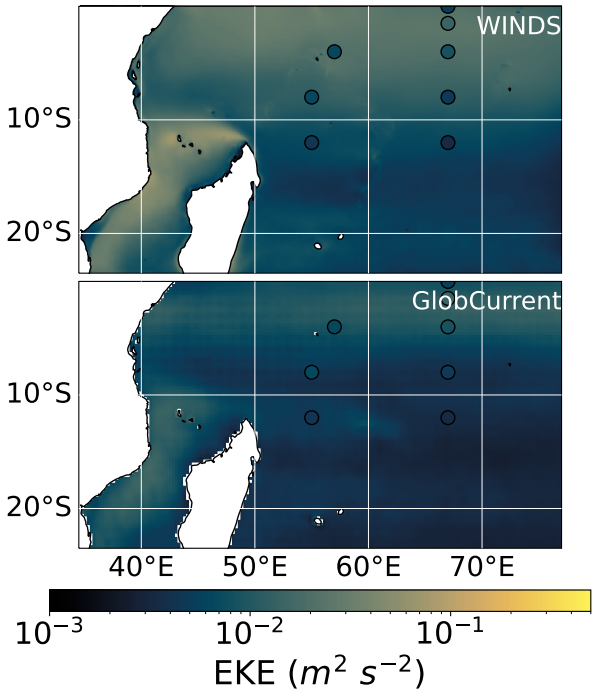

Figure 5. Eddy kinetic energy (EKE) from WINDS (top) and Copernicus GlobCurrent (bottom). EKE was computed by passing daily-mean surface velocity through a high-pass filter with a cutoff period of 30 days, thereby removing high-frequency variability associated with tides, and low-frequency variability associated with time-mean currents and the seasonal cycle. Circles represent the EKE at 10/12 m depth from the RAMA array. EKE is also plotted as a monthly climatology in Figures S1-S3, and MKE (annual-mean and monthly-climatological) in Figures S4-S7.

ARMOR3D does not fully capture the fine-scale freshwater plume associated with the Zambeze River. Figure 9 shows time-series of the difference in SST and SSS between WINDS, and OSTIA and ARMOR3D, across the simulation timespan. Errors in both SST and SSS follow a seasonal cycle (as indicated by Figures 7-8) but annual mean SST errors are relatively consistent from 1993-2020. There is a reduction in errors associated with salinity after 2004, however, perhaps due to improvements in the availability of observations for data-assimilation in ERA-5 (setting ocean-atmosphere fluxes in WINDS).

5 Conclusions

WINDS, and specifically the realistic WINDS-M experiment, reproduces surface circulation well in the southwestern Indian Ocean. Although eddies simulated by WINDS may be too energetic in some parts, such as within 5° of the equator, WINDS-M successfully reproduces the main features of surface circulation across the region, as well as surface properties such as temperature and salinity. Although observations of sub-mesoscale circulation in particular in the southwestern Indian Ocean are lacking, our validation of WINDS-M suggests that this product is suitable for model-based studies investigating the dispersal

https://doi.org/10.5194/gmd-2022-228
Preprint. Discussion started: 10 November 2022

Geoscientific Model Development Discussions
Open Access
EGU

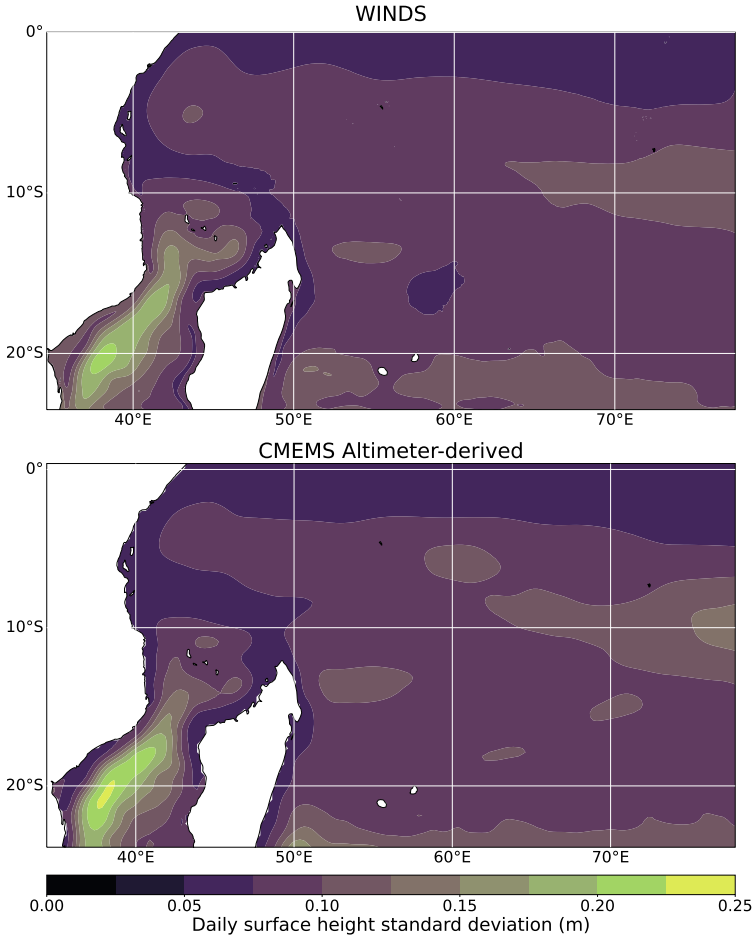

Figure 6. Variability of sea-surface height from 1993-2020 from WINDS (top) and the CMEMS Global Ocean Reprocessed Gridded L4 sea-surface Height product (bottom), computed as a standard deviation.

of buoyant particles on scales of $\mathcal{O}(10^1 - 10^3)$ km. To our knowledge, the spatial resolution of WINDS-M is a four-fold improvement on the highest resolution publicly available dataset for surface currents in the southwestern Indian Ocean ($1/12°$ global ocean (re)analyses, such as GLORYS12V1 (Lellouche et al., 2021)), and the temporal resolution (30 minutes) is also sufficient to fully capture tidal currents. We hope that the output of WINDS will be useful for those investigating marine dispersal (and, more broadly, marine science) in the southwestern Indian Ocean.

Code and data availability. The full dataset (WINDS-C and WINDS-M), as summarised in section 3, is permanently archived at the British Oceanographic Data Centre:

– **WINDS-C**: http://dx.doi.org/10.5285/b2b9bfe408f14ea7a79d9ff7aee0d0b8

https://doi.org/10.5194/gmd-2022-228
Preprint. Discussion started: 10 November 2022

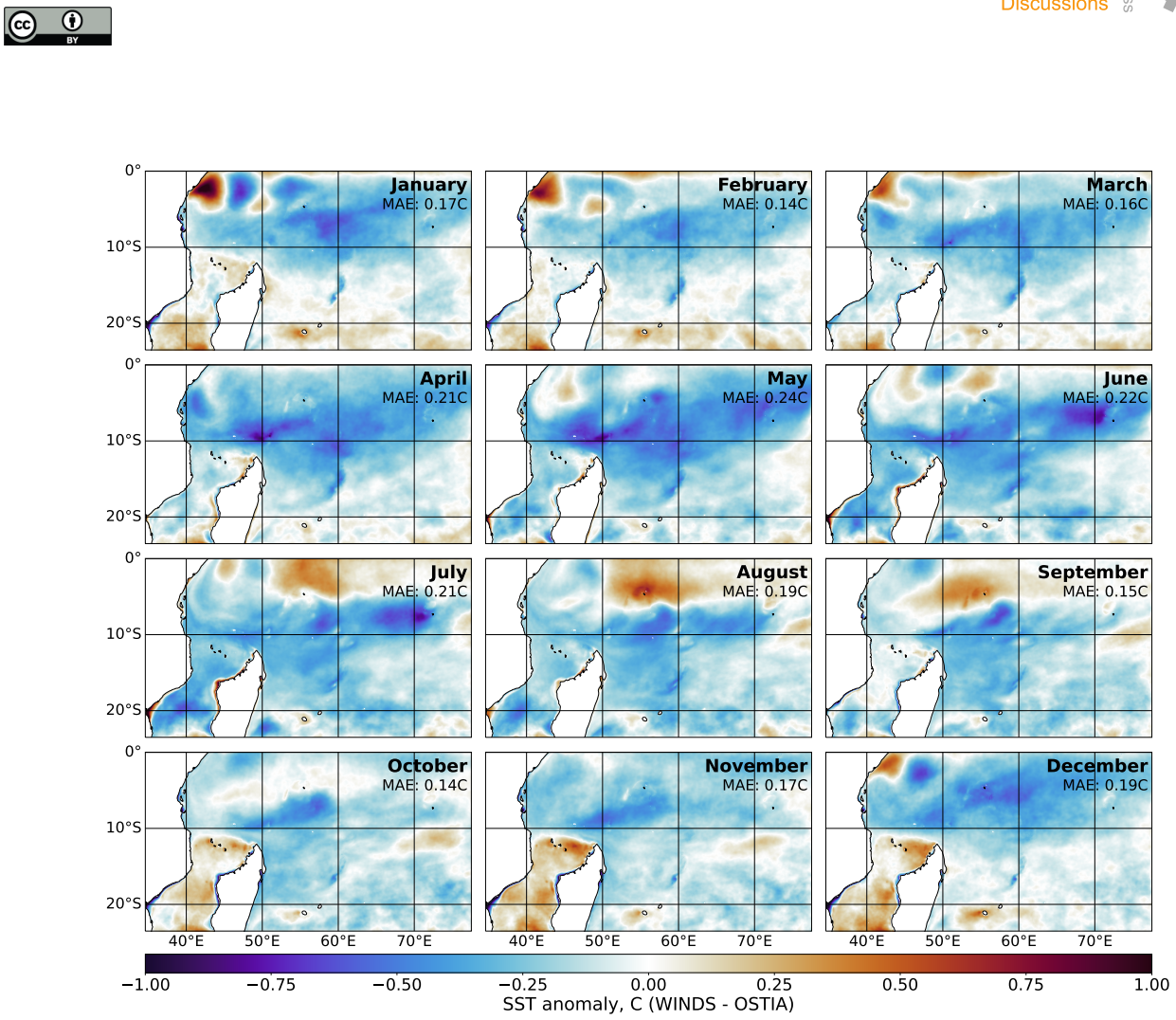

Figure 7. Difference between monthly climatological SST simulated by WINDS, and satellite and in-situ derived SST estimates from OSTIA. Blues indicate that WINDS simulates cooler temperatures, reds indicate that WINDS is warmer.

– **WINDS-M**: http://dx.doi.org/10.5285/BF6F0CFBD09E47498572F21081376702

We have also provided the CROCO configuration files that were used to run WINDS, as well as the model grid, and forcing files used by WINDS-C (the forcing files used by WINDS-M were too large to store permanently, but are described in sections 2.5 and 2.6). The configuration files and code required to reproduce figures in this manuscript are archived at https://dx.doi.org/10.5281/zenodo.7186244.

CROCO V1.1 is available to download at https://data-croco.ifremer.fr/CODE_ARCHIVE/croco-v1.1.tar.gz.

Video supplement. Supplementary video 1: visualisation of 1 year of surface temperatures from WINDS-C Year 8, at daily resolution, generated for outreach purposes. Surface temperature is rendered as a heightmap for this visualisation to highlight flow, and the colourmap range is 22-30°C.

https://doi.org/10.5194/gmd-2022-228
Preprint. Discussion started: 10 November 2022

Geoscientific Model Development Discussions
Open Access
EGU

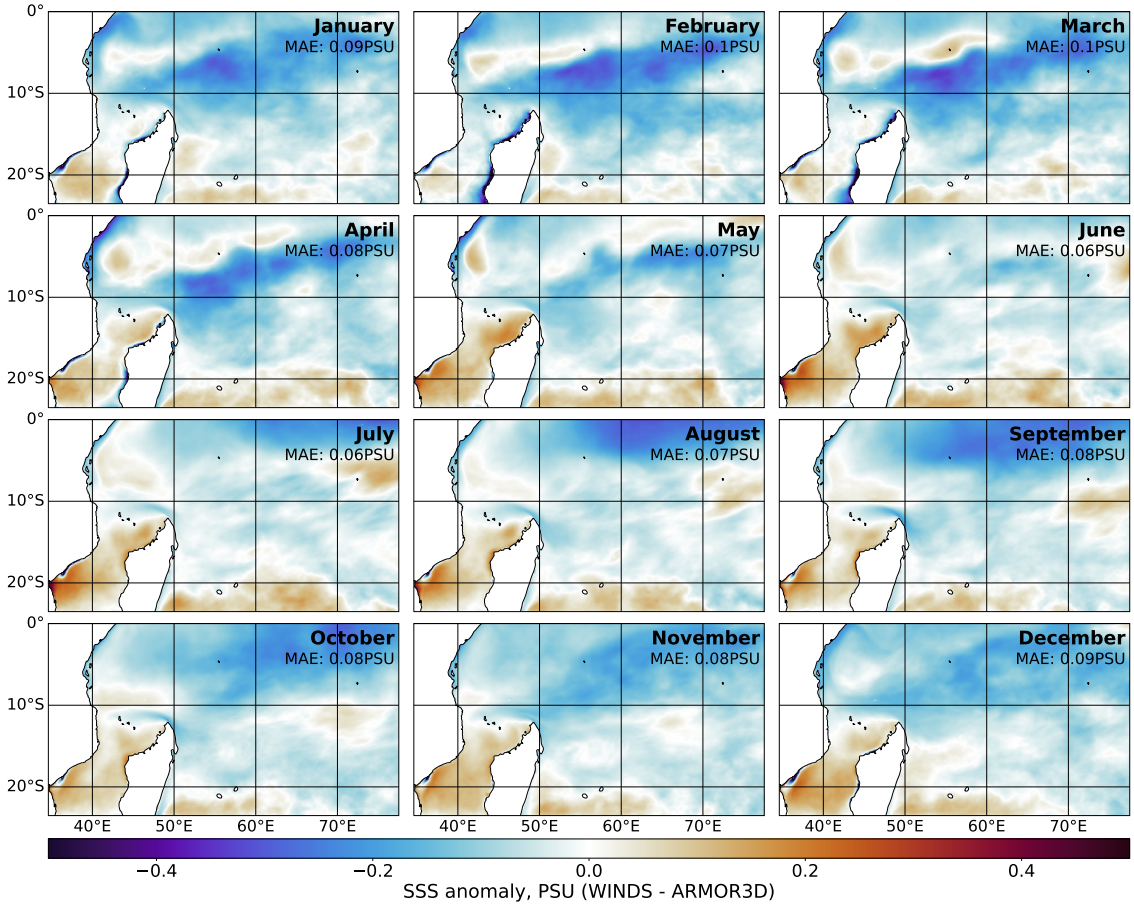

Figure 8. Difference between monthly climatological SSS simulated by WINDS, and in-situ derived SSS estimates from ARMOR3D. Blues indicate that WINDS simulates lower salinity (fresher), reds indicate that WINDS simulates higher salinity (saltier).

Author contributions. NV: *Conceptualisation, methodology, software, validation, writing (original draft), visualisation, funding acquisition.* HJ: *Conceptualisation, methodology, resources, supervision, funding acquisition.*

Competing interests. The authors declare that they have no known competing interests that could have appeared to influence the work reported in this paper.

Acknowledgements. This work was funded by NERC grant NE/S007474/1, and used the ARCHER2 UK National Supercomputing Service (https://www.archer2.ac.uk) and JASMIN, the UK collaborative data analysis facility. CROCO and CROCO_TOOLS are provided by http://www.croco-ocean.org.

https://doi.org/10.5194/gmd-2022-228
Preprint. Discussion started: 10 November 2022

Geoscientific Model Development Discussions

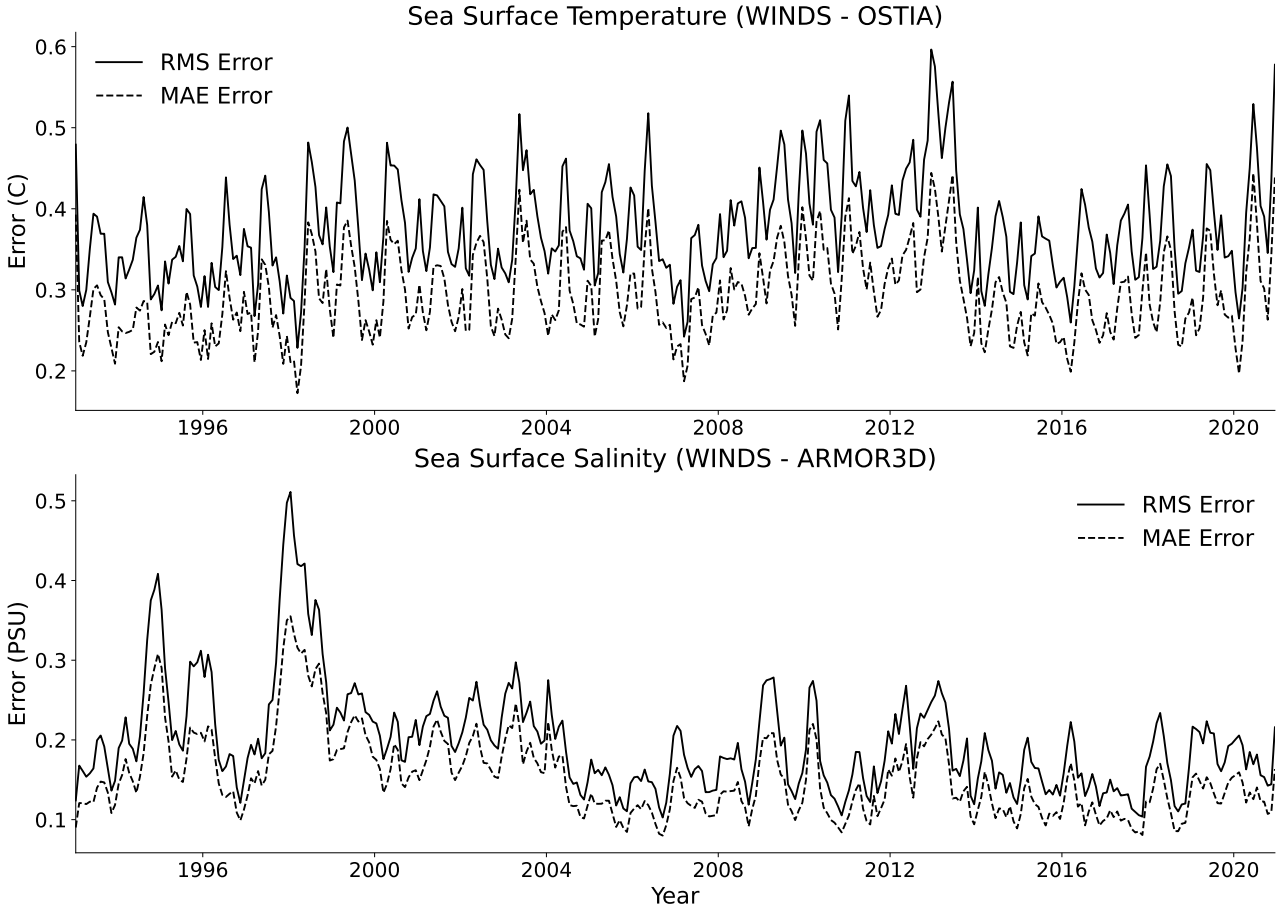

Figure 9. *Top*: Root mean square (RMS) and mean absolute error (MAE) between monthly averages of WINDS and OSTIA from 1993-2020.
Top: Root mean square (RMS) and mean absolute error (MAE) between monthly averages of WINDS and OSTIA from 1993-2020.

References

Beal, L. M., Vialard, J., and Roxy, M. K.: Full Report. IndOOS-2: A roadmap to sustained observations of the Indian Ocean for 2020-2030, http://www.clivar.org/sites/default/files/documents/IndOOS_report_small.pdf, 2019.

Dai, A. and Trenberth, K. E.: Estimates of freshwater discharge from continents: Latitudinal and seasonal variations, Journal of Hydrometeorology, 3, 660–687, https://doi.org/https://doi.org/10.1175/1525-7541(2002)003<0660:EOFDFC>2.0.CO;2, 2002.

Dauhajre, D. P., McWilliams, J. C., and Renault, L.: Nearshore Lagrangian Connectivity: Submesoscale Influence and Resolution Sensitivity, Journal of Geophysical Research: Oceans, 124, 5180–5204, https://doi.org/10.1029/2019JC014943, 2019.

Dunne, R.: Tides and sea level in the Chagos Archipelago, Tech. Rep. September, https://sites.google.com/site/thechagosarchipelago2/chagos-science/sea-level/tides-sea-level-2021, 2021.

Edmunds, P. J., McIlroy, S. E., Adjeroud, M., Ang, P., Bergman, J. L., Carpenter, R. C., Coffroth, M. A., Fujimura, A. G., Hench, J. L., Holbrook, S. J., Leichter, J. J., Muko, S., Nakajima, Y., Nakamura, M., Paris, C. B., Schmitt, R. J., Sutthacheep, M., Too-

https://doi.org/10.5194/gmd-2022-228
Preprint. Discussion started: 10 November 2022

nen, R. J., Sakai, K., Suzuki, G., Washburn, L., Wyatt, A. S. J., and Mitarai, S.: Critical Information Gaps Impeding Understanding of the Role of Larval Connectivity Among Coral Reef Islands in an Era of Global Change, Frontiers in Marine Science, 5, 1–16, https://doi.org/10.3389/fmars.2018.00290, 2018.

Egbert, G. D. and Erofeeva, S. Y.: Efficient inverse modeling of barotropic ocean tides, Journal of Atmospheric and Oceanic Technology, 19, 183–204, https://doi.org/10.1175/1520-0426(2002)019<0183:EIMOBO>2.0.CO;2, 2002.

GEBCO Compilation Group: GEBCO 2019 Grid, https://doi.org/10.5285/836f016a-33be-6ddc-e053-6c86abc0788e, 2019.

Good, S., Fiedler, E., Mao, C., Martin, M. J., Maycock, A., Reid, R., Roberts-Jones, J., Searle, T., Waters, J., While, J., and Worsfold, M.: The current configuration of the OSTIA system for operational production of foundation sea surface temperature and ice concentration analyses, Remote Sensing, 12, 1–20, https://doi.org/10.3390/rs12040720, 2020.

Grimaldi, C. M., Lowe, R. J., Benthuysen, J. A., Cuttler, M. V. W., Green, R. H., Radford, B., Ryan, N., and Gilmour, J.: Hydrodynamic drivers of fine-scale connectivity within a coral reef atoll, Limnology and Oceanography, pp. 1–14, https://doi.org/10.1002/lno.12198, 2022.

Guinehut, S., Dhomps, A. L., Larnicol, G., and Le Traon, P. Y.: High resolution 3-D temperature and salinity fields derived from in situ and satellite observations, Ocean Science, 8, 845–857, https://doi.org/10.5194/os-8-845-2012, 2012.

Hersbach, H., Bell, B., Berrisford, P., Hirahara, S., Horányi, A., Muñoz-Sabater, J., Nicolas, J., Peubey, C., Radu, R., Schepers, D., Simmons, A., Soci, C., Abdalla, S., Abellan, X., Balsamo, G., Bechtold, P., Biavati, G., Bidlot, J., Bonavita, M., De Chiara, G., Dahlgren, P., Dee, D., Diamantakis, M., Dragani, R., Flemming, J., Forbes, R., Fuentes, M., Geer, A., Haimberger, L., Healy, S., Hogan, R. J., Hólm, E., Janisková, M., Keeley, S., Laloyaux, P., Lopez, P., Lupu, C., Radnoti, G., de Rosnay, P., Rozum, I., Vamborg, F., Villaume, S., and Thépaut, J. N.: The ERA5 global reanalysis, Quarterly Journal of the Royal Meteorological Society, 146, 1999–2049, https://doi.org/10.1002/qj.3803, 2020.

Jackett, D. R. and Mcdougall, T. J.: Minimal Adjustment of Hydrographic Profiles to Achieve Static Stability, Journal of Atmospheric and Oceanic Technology, 12, 381–389, https://doi.org/10.1175/1520-0426(1995)012<0381:MAOHPT>2.0.CO;2, 1995.

Jones, W. and Launder, B.: The prediction of laminarization with a two-equation model of turbulence, International Journal of Heat and Mass Transfer, 15, 301–314, https://doi.org/10.1016/0017-9310(72)90076-2, 1972.

Laurindo, L. C., Mariano, A. J., and Lumpkin, R.: An improved near-surface velocity climatology for the global ocean from drifter observations, Deep-Sea Research Part I: Oceanographic Research Papers, 124, 73–92, https://doi.org/10.1016/j.dsr.2017.04.009, 2017.

Lellouche, J.-M., Greiner, E., Bourdallé Badie, R., Garric, G., Melet, A., Drévillon, M., Bricaud, C., Hamon, M., Le Galloudec, O., Regnier, C., Candela, T., Testut, C.-E., Gasparin, F., Ruggiero, G., Benkiran, M., Drillet, Y., and Le Traon, P.-Y.: The Copernicus Global 1/12° Oceanic and Sea Ice GLORYS12 Reanalysis, Frontiers in Earth Science, 9, 1–27, https://doi.org/10.3389/feart.2021.698876, 2021.

Lowry, R., Pugh, D., and Wijeratne, E.: Observations of Seiching and Tides Around the Islands of Mauritius and Rodrigues, Western Indian Ocean Journal of Marine Science, 7, https://doi.org/10.4314/wiojms.v7i1.48251, 2009.

Mayorga-Adame, C. G., Ted Strub, P., Batchelder, H. P., and Spitz, Y. H.: Characterizing the circulation off the Kenyan-Tanzanian coast using an ocean model, Journal of Geophysical Research: Oceans, 121, 1377–1399, https://doi.org/10.1002/2015JC010860, 2016.

Mayorga-Adame, C. G., Batchelder, H. P., and Spitz, Y. H.: Modeling larval connectivity of coral reef organisms in the Kenya-Tanzania region, Frontiers in Marine Science, 4, https://doi.org/10.3389/fmars.2017.00092, 2017.

McPhaden, M. J., Meyers, G., Ando, K., Masumoto, Y., Murty, V. S., Ravichandran, M., Syamsudin, F., Vialard, J., Yu, L., and Yu, W.: RAMA: The research moored array for African-Asian-Australian monsoon analysis and prediction, Bulletin of the American Meteorological Society, 90, 459–480, https://doi.org/10.1175/2008BAMS2608.1, 2009.

https://doi.org/10.5194/gmd-2022-228
Preprint. Discussion started: 10 November 2022

Monismith, S. G., Barkdull, M. K., Nunome, Y., and Mitarai, S.: Transport Between Palau and the Eastern Coral Triangle: Larval Connectivity or Near Misses, Geophysical Research Letters, 45, 4974–4981, https://doi.org/10.1029/2018GL077493, 2018.

Painter, S. C.: The biogeochemistry and oceanography of the East African Coastal Current, Progress in Oceanography, 186, 102 374, https://doi.org/10.1016/j.pocean.2020.102374, 2020.

Pugh, D.: Sea levels at Aldabra Atoll, Mombasa and Mahé, western equatorial Indian Ocean, related to tides, meteorology and ocean circulation, Deep Sea Research Part A, Oceanographic Research Papers, 26, 237–258, https://doi.org/10.1016/0198-0149(79)90022-0, 1979.

Rio, M. H., Mulet, S., and Picot, N.: Beyond GOCE for the ocean circulation estimate: Synergetic use of altimetry, gravimetry, and in situ data provides new insight into geostrophic and Ekman currents, Geophysical Research Letters, 41, 8918–8925, https://doi.org/10.1002/2014GL061773, 2014.

Schott, F. A. and McCreary, J. P.: The monsoon circulation of the Indian Ocean, Progress in Oceanography, 51, 1–123, https://doi.org/10.1016/S0079-6611(01)00083-0, 2001.

Schott, F. A., Xie, S. P., and McCreary, J. P.: Indian ocean circulation and climate variability, Reviews of Geophysics, 47, 1–46, https://doi.org/10.1029/2007RG000245, 2009.

Shao-Jun, Z., Yu-Hong, Z., Wei, Z., Jia-Xun, L., and Yan, D.: Typical Surface Seasonal Circulation in the Indian Ocean Derived from Argos Floats, Atmospheric and Oceanic Science Letters, 5, 329–333, https://doi.org/10.1080/16742834.2012.11447015, 2012.

Shchepetkin, A. F. and McWilliams, J. C.: A method for computing horizontal pressure-gradient force in an oceanic model with a nonaligned vertical coordinate, Journal of Geophysical Research: Oceans, 108, 1–34, https://doi.org/10.1029/2001jc001047, 2003.

Shchepetkin, A. F. and McWilliams, J. C.: The regional oceanic modeling system (ROMS): A split-explicit, free-surface, topography-following-coordinate oceanic model, Ocean Modelling, 9, 347–404, https://doi.org/10.1016/j.ocemod.2004.08.002, 2005.

Smagorinsky, J.: GENERAL CIRCULATION EXPERIMENTS WITH THE PRIMITIVE EQUATIONS, Monthly Weather Review, 91, 99–164, https://doi.org/10.1175/1520-0493(1963)091<0099:GCEWTP>2.3.CO;2, 1963.

Swallow, J., Fieux, M., and Schott, F.: The boundary currents east and north of Madagascar: 1. Geostrophic currents and transports, Journal of Geophysical Research, 93, 4951, https://doi.org/10.1029/jc093ic05p04951, 1988.

Swallow, J. C., Schott, F., and Fieux, M.: Structure and transport of the East African Coastal Current, Journal of Geophysical Research, 96, 22 245, https://doi.org/10.1029/91jc01942, 1991.

Thompson, D. M., Kleypas, J., Castruccio, F., Curchitser, E. N., Pinsky, M. L., Jönsson, B., and Watson, J. R.: Variability in oceanographic barriers to coral larval dispersal: Do currents shape biodiversity?, Progress in Oceanography, 165, 110–122, https://doi.org/10.1016/j.pocean.2018.05.007, 2018.

Tozer, B., Sandwell, D. T., Smith, W. H., Olson, C., Beale, J. R., and Wessel, P.: Global Bathymetry and Topography at 15 Arc Sec: SRTM15+, Earth and Space Science, 6, 1847–1864, https://doi.org/10.1029/2019EA000658, 2019.

van Sebille, E., Griffies, S. M., Abernathey, R., Adams, T. P., Berloff, P., Biastoch, A., Blanke, B., Chassignet, E. P., Cheng, Y., Cotter, C. J., Deleersnijder, E., Döös, K., Drake, H. F., Drijfhout, S., Gary, S. F., Heemink, A. W., Kjellsson, J., Koszalka, I. M., Lange, M., Lique, C., MacGilchrist, G. A., Marsh, R., Mayorga Adame, C. G., McAdam, R., Nencioli, F., Paris, C. B., Piggott, M. D., Polton, J. A., Rühs, S., Shah, S. H., Thomas, M. D., Wang, J., Wolfram, P. J., Zanna, L., and Zika, J. D.: Lagrangian ocean analysis: Fundamentals and practices, https://doi.org/10.1016/j.ocemod.2017.11.008, 2018.

Voldsund, A., Aguiar-González, B., Gammelsrød, T., Krakstad, J. O., and Ullgren, J.: Observations of the east Madagascar current system: Dynamics and volume transports, Journal of Marine Research, 75, 531–555, https://doi.org/10.1357/002224017821836725, 2017.

https://doi.org/10.5194/gmd-2022-228
Preprint. Discussion started: 10 November 2022

Wessel, P. and Smith, W. H. F.: A global, self-consistent, hierarchical, high-resolution shoreline database, Journal of Geophysical Research: Solid Earth, 101, 8741–8743, https://doi.org/10.1029/96jb00104, 1996.